ELSEVIER
Available online at www.sciencedirect.com
ScienceDirect
Journal of Hydro-environment Research xx (2013) 1−14
Journal of Hydro-environment Research
www.elsevier.com/locate/jher

Physical-scale model designs for engineered log jams in rivers

Michael S. Gallisdorfer [a], Sean J. Bennett [a,*], Joseph F. Atkinson [b], S. Mohammad Ghaneeizad [b], Andrew P. Brooks [c], Andrew Simon [d], Eddy J. Langendoen [e]

[a] *Department of Geography, University at Buffalo, Buffalo, NY 14261-0055, USA*
[b] *Department of Civil, Structural, and Environmental Engineering, University at Buffalo, Buffalo, NY 14260, USA*
[c] *Australian Rivers Institute, Griffith University, Nathan, QLD 4111, Australia*
[d] *CardnoENTRIX, 1223 Jackson Avenue East, Suite 301, Oxford, MS 38655, USA*
[e] *USDA-ARS National Sedimentation Laboratory, Oxford, MS, 38655, USA*

Received 4 November 2012; revised 7 October 2013; accepted 15 October 2013

Abstract

Stream restoration and river engineering projects are employing engineered log jams (ELJs) increasingly for stabilization and in-stream improvements. To advance the design of these structures and to evaluate their morphodynamic effects on corridors, the basis for physical-scale models of rivers with ELJs is presented and discussed. The prototype selected is the Big Sioux River, SD, chosen because ELJs will be used to mitigate excessive bank erosion. The underlying theory of physical-scale modeling and all primary and secondary scaling ratios are presented for two boundary conditions, a fixed- and movable-bed, given the experimental constraints of the intended facility. The scaling ratios for the movable-bed model sediment are relaxed, allowing for the use of typical experimental flows, facilities, and materials. Proposed ELJ designs are based on proven field installations, and these structures also are scaled to natural timber dimensions to be used in the prototype. Preliminary results from these physical models show that (1) ELJs greatly decelerate flow near the structure and accelerate flow in the main portion of the channel, yet spatially averaged flow velocity and depth remain unchanged, (2) derived drag coefficients for the ELJs based on force measurements vary from 0.3 to 0.7 depending on the scaling velocity employed, and (3) while significant localized erosion and deposition occurred in the vicinity of the ELJ, these effects extended well downstream of the structure and across the entire channel. Although physical experimentation using wood is not uncommon, the use of physical scaling theory appears to be employed infrequently, which potentially could limit the applicability of the results obtained. It is envisioned that the procedures outlined here would become more widely used in experimental research of rivers and in river restoration design.

© 2013 International Association for Hydro-environment Engineering and Research, Asia Pacific Division. Published by Elsevier B.V. All rights reserved.

Keywords: Engineered log jams; Physical-scale model; Bank protection; Drag forces

1. Introduction

Stream restoration and river engineering projects often use in-stream structures to stabilize stream banks, to redirect and dissipate flow energy, and to provide geomorphic and ecosystem services to the corridor (Bernhardt et al., 2005). While many of these in-stream structures are composed of rock, the use of wood, large woody debris, and engineered log jams (ELJs) have increased considerably (Shields et al., 2004; Brooks, 2006; Abbe and Brooks, 2011). ELJs now represent an ecologically sensitive and multifunctional alternative to in-stream structures composed of conventional materials (Abbe et al., 2003b; Brooks, 2006).

The reintroduction of large wood, as ELJs, to degraded rivers affords many benefits to these impaired corridors. With ELJs, there exists the potential to restore critical ecological attributes and to re-initiate dampened or absent physical and biological processes while simultaneously performing traditional

---

* Corresponding author. Tel.: +1 716 645 0490.
E-mail address: seanb@buffalo.edu (S.J. Bennett).

1570-6443/$ - see front matter © 2013 International Association for Hydro-environment Engineering and Research, Asia Pacific Division. Published by Elsevier B.V. All rights reserved.

Please cite this article in press as: Gallisdorfer, M.S., et al., Physical-scale model designs for engineered log jams in rivers, Journal of Hydro-environment Research (2013), http://dx.doi.org/10.1016/j.jher.2013.10.002

functions of in-stream structures (Abbe et al., 2003a; Brooks, 2006). Engineered log jams have been deployed successfully to protect vulnerable banks while increasing channel complexity and habitat resources (Abbe et al. 2003a,b). Organic matter and sediment often can be sequestered effectively by artificial debris jams (Flores et al., 2011), demonstrating their functional similarity to natural wood jams (Shields et al., 2008). Flume studies investigating the effects of large wood (LW) on hyporheic processes suggest that these structures may be capable of driving and enhancing local flow exchange (Mutz et al., 2007). The use of ELJs in degraded rivers also may accelerate ecological recovery by initiating the redevelopment of geomorphic, hydraulic, and ecological complexity when riparian services are either absent or decoupled from the stream channel (Brooks, 2006; Collins et al., 2012). It is well known that the historical removal of large wood from rivers has resulted in physical and ecological degradations, with increased stream power and decreased channel roughness, and reductions in sediment retention, habitat area, and channel complexity (Shields and Gippel, 1995; Abbe and Montgomery, 1996; Abbe et al., 2003a,b; Brooks, 2006). As such, the introduction of large wood can positively influence the long-term dynamic stability and integrity of fluvial landscapes (Collins et al., 2012).

While some design criteria exist, important gaps still remain in the understanding, implementation, and long-term effects of ELJs on river morphodynamics. Detailed descriptions of design criteria for large woody debris and ELJs, including their construction and installation guidelines, are reviewed in D’Aoust and Millar (2000), Shields et al. (2004), Brooks (2006) and Abbe and Brooks (2011). A recent workshop, however, identified that critical research needs for the use of large wood in river restoration (U.S. Bureau of Reclamation and U.S. Army Corps of Engineers, 2012). One approach to address these technical needs, as identified therein, is the use of physical models, which is the focus of the current paper.

Employing physical models to assess large wood and woody debris in rivers is not a new concept. Table 1 lists many such successful experimental campaigns, highlighting the facilities used, the boundary conditions considered, and the phenomena examined. These studies have provided much insight into how experimental river channels can entrain and transport wood and how the introduction of wood causes localized erosion and deposition and alterations to time-mean and turbulent flow, bed shear stress, flow resistance, and hyporheic flow exchange. Many of these flume studies, however, did not employ scaling principles often used in physical models to link unambiguously the results of the laboratory experiment to a field prototype. This may not have been necessary, since several of these studies were conducted to explore the general interactions of flow and bed morphology with vegetation, rather than specific responses within an identified field prototype. Yet, by not employing scaling principles, the application or interpretation of these experimental results in natural settings may be problematic. This is because the imposed distortions in scale in the physical model may be unknown or poorly defined, and these distortions could amplify or suppress the observations recorded as compared to the natural river.

The present study is part of a research program that seeks to understand further the morphodynamic response of rivers to the introduction of ELJs, to enhance and refine the design criteria and resiliency of these structures for use in river restoration projects, and to maximize the ecologic and geomorphic benefits of ELJs at various scales within actively managed river systems. The objectives of the present study are to (1) review the theory employed in the scaling and construction of physical river models, so that experimental drag measurements can be scaled to prototype conditions, (2) design physical-scale models with fixed- and movable-beds with ELJs, and (3) present preliminary results from the experimental campaign. The Big Sioux River in South Dakota, USA, was selected as the field prototype because local stakeholders, working with state and federal agencies, are seeking to reduce suspended sediment and nutrient loads caused by excessive bank erosion (S. Brich, pers. comm.). As such, these stakeholders intend to install ELJs at discrete locations to reduce this erosion. The emphasis here is placed on the principles of physical model construction for a prototypical river with ELJs. It is envisioned that the procedures presented will be more commonly employed by experimentalists conducting research on wood in river corridors, thereby broadening significantly the applicability of the results obtained.

2. Prototype description

The Big Sioux River flows 676 km from its headwaters in northern South Dakota, USA, through Iowa to its juncture with the Missouri River, near Sioux City, IA, draining a watershed of approximately 24,790 km^2. Its mean annual flow Q_{ma} is 12.7 m^3 s^{-1} and its 1.5 ($Q_{1.5}$) and 2.33 ($Q_{2.33}$) year return flows are 57.5 m^3 s^{-1} and 93.4 m^3 s^{-1}, respectively, as determined by flow-frequency analysis for data collected near Dell Rapids, SD (USGS 06481000; Fig. 1). Using available channel cross-sectional data (S. Brich, pers. comm.), the following parameters are derived for the prototype: mean channel surface width w of 40.5 m, a mean flow depth h of 2.2 m, a mean water surface slope S_S of 0.00040, and a mean bed slope S_B of 0.00047. Based on $Q_{1.5}$ and mean channel cross-sectional area A, a mean flow velocity v of 0.645 m s^{-1} and a Froude number Fr of 0.124 are determined, where

$$\mathrm{Fr} = v/\sqrt{gh} \tag{1}$$

and g is gravitational acceleration. Median grain size of the bed D_{50} varies from 0.1 mm at 1.6 km east of Dell Rapids to 0.08 mm at 1.9 km south (D. Vockrodt, pers. comm.). These prototype channel dimensions and the hydraulic and sediment grain size parameters are used to construct the physical models described below.

3. Theory of hydraulic modeling: brief review

To achieve complete mechanical similitude to a prototype river, a physical model must display geometric, kinematic, and dynamic similitude to that system (Yalin, 1971; Wallerstein

Please cite this article in press as: Gallisdorfer, M.S., et al., Physical-scale model designs for engineered log jams in rivers, Journal of Hydro-environment Research (2013), http://dx.doi.org/10.1016/j.jher.2013.10.002

Table 1
Summary of select studies employing physical models to examine large wood (LW) behavior in rivers.

Study	Use of a prototype stream	Scaling	Model dimensions: width, depth, length (m)	Bed type; D_{50} (mm)	Flow rate ($m^3\ s^{-1}$)	Flow depth (m)	LW model composition and description	LW dimensions: diameter, length (m)	Phenomena investigated
Beschta (1983)	No	NA	0.132, 0.6, 10	Movable-bed; 54	0.001–0.027	0.27–0.55	Metal cylinder; trunk	0.06–0.20, NA	Effect of LW on bed morphology
Cherry and Beschta (1989)	No	NA	0.40, NA, 6.1	Movable-bed; 0.04	0.001–0.003	0.012–0.02	Wooden dowel; trunk	0.0127, NA	Effect of LW orientation on bed morphology
Young (1991)	No	Fr	0.46, 0.27, 8	Fixed-bed	0.0041	0.1	Wooden dowel; trunk	0.013–0.025, 0.225–0.450	Effect of LW abundance on flood level
Gippel et al. (1992)	No	NA	Tow-tank: 2, 2, NA; Channel: 0.6, NA, NA	Na	0.037–0.082 (flume)	2 (tow-tank); 0.1–0.25 (flume)	PVC cylinder(s), branched; trunk(s)	0.048–0.076, 0.125–0.455	LW drag coefficients, and effects of shielding and blockage
Braudrick et al. (1997)	No	NA	1, NA, 15	Movable-bed; 1	0.0045–0.012	0.015–0.027	Wooden dowels; trunks	0.02–0.04, 0.2–0.4	Wood transport dynamics
Beebe (2000)	No	NA	0.63, NA, 10	Movable-bed; 0.04	0.008–0.022	0.065–0.126	Log; bark and branches	0.063, 0.582	Effect of LW on flow
Braudrick and Grant (2000, 2001)	No	NA	1.22, NA, 9.14	Fixed-bed; 8	0.008–0.011	0.015–0.020	Wooden dowel; trunk, some with rootwad	0.025–0.038, 0.30–0.60	Entrainment of individual logs
Wallerstein et al. (2001)	Yes	Fr	0.63, 0.61, 10	Movable-bed; 8	0.003	0.07	Wooden dowels; trunks as LWD	0.019, 0.07–0.3	Effect of LW on channel hydraulics and morphology
Wallerstein et al. (2002)	Yes	Fr	1.2, 0.3, 25	Fixed-bed	0.076 (mean)	0.30 (mean)	Aluminum cylinder	0.019, 0.07–0.3	Drag forces acting on LW
Alonso et al. (2005, 2009); Shields and Alonso (2012)	No	At scale	1.8, 0.8, 137	Grass	2.07–3.43	0.80–0.85	PVC cylinder, logs; trunk	0.22, 1.80	Drag and lift forces acting on LW
Bocchiola et al. (2006)	No	NA	1, NA, 30	Fixed-bed; 2 and 5	0.0031–0.045 (sliding); 0.0003–0.019 (rolling)	0.015–0.068 (sliding); 0.004–0.100 (rolling)	Wooden dowel; trunk	0.03–0.1, 0.25–0.50	Entrainment of LW
Wilcox et al. (2006); Wilcox and Wohl (2006)	No	NA	0.6, NA, 10	Fixed-bed; 15	0.004–0.064	0.01–0.14	PVC cylinders, wooden blocks; trunk with rootwad	0.025–0.038, 0.3–0.6	Effect of LW on flow resistance
Bocchiola (2011)	No	NA	1, NA, 30	Fixed-bed; 1.8	0.0011–0.0200	0.008–0.050	Wooden dowels; trunks	0.006–0.026, 0.05–0.30	Effect of LW reintroduction on channel parameters
Svoboda and Russel (2011)	No	Fr	2.7, NA, 9	Movable-bed; 8	0.034–0.24	0.056–0.170	Wooden dowel; trunk and rootwad as LWD	0.091–0.183; 1.40	Effect of LW on bed morphology

Please cite this article in press as: Gallisdorfer, M.S., et al., Physical-scale model designs for engineered log jams in rivers, Journal of Hydro-environment Research (2013), http://dx.doi.org/10.1016/j.jher.2013.10.002

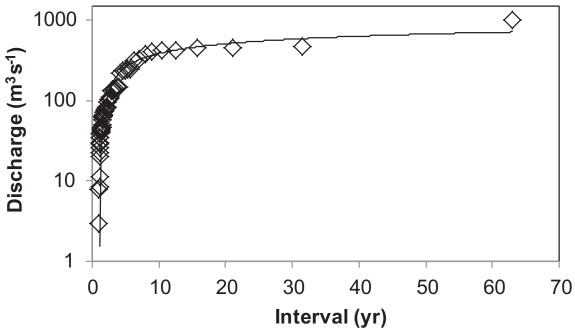

Fig. 1. Flow-frequency analysis for the Big Sioux River near Dell Rapids, SD (USGS 06481000).

et al., 1999, 2001; Julien, 2002; Heller, 2011). Geometric similitude results when the ratios of all geometric dimensions of the prototype (denoted by subscript p) and model (denoted by subscript m) are scaled congruently. Kinematic similitude results when model particle path lengths and travel times occur in proportion to the prototype. Dynamic similitude results when forces acting in a model are scaled proportionally to those acting in the prototype. Resulting scaling ratios (prototype-to-model, denoted by subscript r) allow experimentalists to examine the hydraulic and morphodynamic behavior of rivers at the laboratory scale and to extrapolate the results to the prototype.

3.1. Dimensional analysis and scaling ratios

The current experimental effort is aimed at measuring drag forces expected to be exerted on the ELJ in the prototype and in quantifying the morphodynamic response of the channel to ELJs. The variables assumed to affect the overall drag are listed in Table 2.

The Buckingham π theorem then can be used to identify the dimensionless parameters of the system and to guide organization of the important variables that need to be considered in constructing physical-scaled models (White, 1994; Wallerstein et al., 1999, 2001). For the present case, 12 variables (drag force F_D in addition to those in Table 2) encompassing three dimensional units (mass M, length L, and time T) lead to the possible need for nine dimensionless parameters. Seven of these characterize general phenomena in open-channel flow (pressure, flow velocity, flow length scale, fluid density, fluid viscosity, fluid surface tension, and gravity), while the remaining variables are added relating to force calculations for the ELJ. This list can be simplified by considering F_D and A_D as the ratio F_D/A_D. In addition, the ELJ is assumed to have a height that is always greater than the water depth (L_s is not necessary) and to be functionally inflexible, which justifies the omission of Young's modulus. Based on the remaining variables, seven dimensionless parameters should be found. Using ρ, v, and L as repeating variables, the following dimensionless relationship may be written:

$$f\left[\frac{F_D}{\rho A_D v^2}, \frac{v}{\sqrt{gL}}, \frac{\rho v L}{\mu}, \frac{\rho v^2 L}{\delta}, \frac{k_{ELJ}}{L}, \beta, \eta\right] = 0$$

or

$$f\left[C_D, \mathrm{Fr}, \mathrm{Re}, \mathrm{We}, \frac{k_{ELJ}}{L}, \beta, \eta\right] = 0 \quad (2)$$

where C_D is a drag coefficient, Re is the Reynolds number, and We is the Weber number (see also Henderson, 1966; Yalin, 1971; White, 1994).

Table 2
Variables used in dimensional analysis.

Symbol	Variable description
A_D	Frontal area of the ELJ with respect to flow direction
L_s	Height of ELJ relative to water depth (i.e., a submergence ratio)
β	A measure of orientation of the ELJ with respect to flow direction
k_{ELJ}	Surface roughness of the ELJ
η	Porosity of the ELJ
v	Flow velocity
ρ	Fluid density
μ	Fluid viscosity
δ	Surface tension
g	Gravity
L	Characteristic length scale

The required model scaling can be simplified further. This can be accomplished by assuming the experiments will preserve the relative orientation of the prototype installation β as well as its porosity η and relative roughness k_{ELJ}/L. The effects of surface tension and viscous forces also may be neglected when the model flow depth h_m is greater than 0.015 m and flow is fully turbulent, so that the main focus for experimental analysis is Fr (Wallerstein et al., 1999). Eq. (2) then reduces to

$$f\left[C_D, \mathrm{Fr}, \left(\frac{k_{ELJ}}{L}, \beta, \eta\right)\right] = 0 \quad (3)$$

This result suggests that the drag coefficient for the model should be the same as the drag coefficient for the prototype so long as the other variables in Eq. (3) are the same.

Froude number scaling is obtained from the following

$$\mathrm{Fr}_r = \frac{\mathrm{Fr}_p}{\mathrm{Fr}_m} = \frac{v_r}{\sqrt{g_r L_r}} = \frac{v_r}{\sqrt{L_r}} = 1 \quad (4)$$

where the gravity ratio g_r is taken to be 1and subscript r denotes a ratio of prototype-to-model value. While maintaining $\mathrm{Fr}_r = 1$, Re scaling is necessarily relaxed when using the same fluid medium. In doing so, it is prudent to increase h_m to ensure fully turbulent flow and to maximize physical space for instrumentation. A consequence of increasing h_m without a corresponding increase in horizontal scale is geometric distortion. As long as the impacts of this distortion can be incorporated into the analysis or neglected, a Fr-scaled physical river model should faithfully simulate forces acting at the field-scale, although neither geometric or full kinematic similarity is strictly maintained. Variation in the longitudinal X_r

Please cite this article in press as: Gallisdorfer, M.S., et al., Physical-scale model designs for engineered log jams in rivers, Journal of Hydro-environment Research (2013), http://dx.doi.org/10.1016/j.jher.2013.10.002

and transverse Y_r length scale ratios is therefore of less concern than variation in the vertical length scale ratio Z_r, which appears in Eq. (1) in place of h.

Additional scaling relationships can be derived for the physical-scale model based upon the general Fr similitude, following Wallerstein et al. (1999, 2001). From Eq. (4),

$$L_r = v_r^2 (= Z_r) \tag{5}$$

The discharge ratio Q_r then becomes

$$Q_r = v_r A_r = \sqrt{L_r} Y_r Z_r = Y_r Z_r^{3/2} = L_r^{5/2} \tag{6}$$

With equal length scale ratios, the slope ratio S_r becomes

$$S_r = \frac{X_r}{Z_r} = 1 \tag{7}$$

and the drag force ratio $(F_D)_r$ becomes

$$(F_D)_r = (C_D)_r \rho_r A_r v_r^2 = (C_D)_r \rho_r L_r^3 = Y_r Z_r^2 \tag{8}$$

assuming $(C_D)_r = 1$ and $\rho_r = 1$.

Consideration of a movable-bed model introduces an additional set of scaling relationships. The dimensionless bed shear stress θ and particle Reynolds number Re_g are defined as:

$$\theta = \frac{\tau_0}{\gamma(\xi - 1)D} \tag{9}$$

and

$$\mathrm{Re}_g = \frac{u^* D}{\nu} \tag{10}$$

where mean boundary shear stress τ_0 and shear velocity u^* are

$$\tau_0 = \gamma R S \tag{11}$$

$$u^* = \sqrt{\tau_0 / \rho} \tag{12}$$

and $\gamma = \rho g$, $\xi = \sigma/\rho$, σ is particle density, D is particle diameter, R is hydraulic radius, and S is slope. Substituting and rearranging Eqs. (9) and (12), and then writing the ratios of each variable in terms of the different length scales yield Einstein and Chien's (1954) scaling ratios for θ_r and $(\mathrm{Re}_g)_r$:

$$\theta_r = \frac{\gamma_r R_r S_r}{\gamma_r (\xi - 1)_r D_r} = \frac{R_r Z_r}{\gamma_{sr} X_r D_r} = 1 \tag{13}$$

$$\left(\mathrm{Re}_g\right)_r = \frac{R_r S_r D_r^2}{\nu_r^2} = \frac{R_r Z_r D_r^2}{\nu_r^2 X_r} = 1 \tag{14}$$

where $\gamma_{sr} = \xi - 1$, $g_r = 1$, and $\gamma_r = 1$. Selecting an appropriate model sediment density and model kinematic viscosity, so that $\theta_r = (\mathrm{Re}_g)_r = 1$, is not possible when using quartz-density sand and fresh water (see Julien, 2002). Pugh (2008) presented an approach to physical modeling of mobile beds based on the relationship between dimensionless bed shear stress θ and the dimensionless unit sediment transport rate. To obtain similarity in sediment transport, this model would employ larger bed sediment of lower density as compared to the prototype.

An appropriate grain size to be used in the model can be determined from these relations. Average bed shear stress for the movable-bed model can be estimated using Eq. (11). With this value, a model sediment grain size D slightly larger than that at the threshold of motion is predicted by Eq. (9) using prescribed values of θ_c, where the subscript c refers to conditions at threshold (see Bridge and Bennett, 1992).

3.2. ELJ scaling ratios

Whereas earlier studies evaluating fluid forces acting on large woody debris (LWD) reported observations for single elements (Table 1), this paper intends to report observations for complex, multi-element models of ELJs scaled to reflect the dimensions of local timber to be used in the prototype. The length scale of individual model timber elements L_T is set equal to the horizontal scale of the movable-bed model, so that the length ratios of all model element dimensions, including element length L_T, trunk diameter D_T, and rootwad diameter RW_T are similar. Model ELJs then are constructed of individual model elements according to conceptual designs used in field applications (see below).

Forces acting on model ELJs can be evaluated in a similar way to those acting on individual elements. The following assumptions are included: (1) flexibility of the ELJs is ignored for practical and theoretical reasons, (2) the Re for both the element and the ELJ are in the fully turbulent domain, and (3) the effects of structural vibrations on F_D are considered negligible (see Naudascher, 1984). The total drag force F_D acting on a model ELJ in the streamwise direction may be calculated according to (see Eqs. (2) and (8))

$$F_D = C_D A_D \frac{\rho v_0^2}{2} \tag{15}$$

where A_D is the projected area of the structure and v_0 is the incident velocity. As indicated in Eq. (3), C_D is related to the Froude number, structure Reynolds number, geometry, orientation, and roughness. In cases where the structure is completely submerged, an additional vertical scale, or submergence factor, would need to be incorporated, as initially included in Table 2 (Alonso, 2004).

4. Physical model design for the Big Sioux River

4.1. Fixed-bed model design

In addition to the scaling considerations discussed above, dimensions of the fixed-bed laboratory model are determined with respect to laboratory space constraints and equipment limitations. The flume model is 1.9 m wide, 0.5 m deep, and 7 m long with 90° fixed banks (Fig. 2). Flow depth is set at 0.11 m to accommodate the fixed flow rate of laboratory equipment while maintaining $F_r = 1$, which is slightly higher than the undistorted fixed-bed model depth of 0.104 m (or Y_r/

Please cite this article in press as: Gallisdorfer, M.S., et al., Physical-scale model designs for engineered log jams in rivers, Journal of Hydro-environment Research (2013), http://dx.doi.org/10.1016/j.jher.2013.10.002

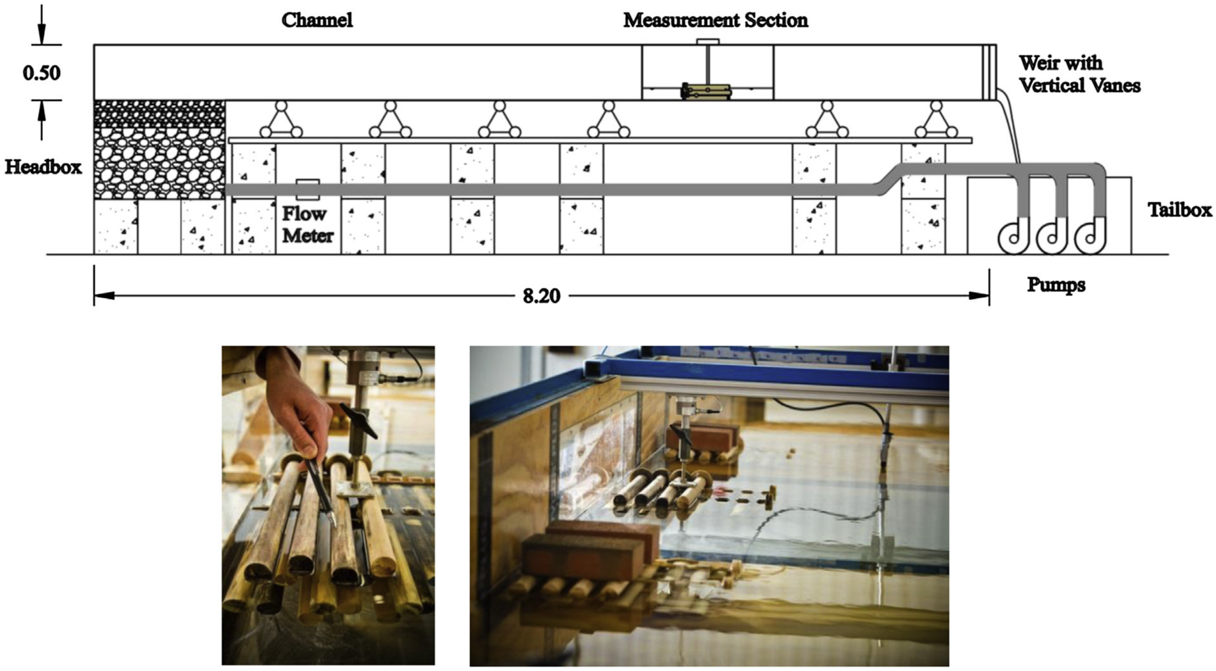

Fig. 2. Schematic and pictures of the experimental facility. The schematic (top) is a cross-sectional view of the flume with flow moving from left to right (dimensions in meters). Looking upstream, the photographs show a close-up of the ELJ connected to the biaxial load cell (bottom left), and three successive ELJs installed along the left bank and the acoustic Doppler velocimeter located near the channel center (bottom right; bricks used as ballast; photographs by D. Levere).

$Z_r = 1.07$). It is also necessary to depart from prototype channel cross-sectional geometry by creating a model with vertical stream banks. All scaling ratios for the fixed-model are determined once these resource, equipment, and space constraints have been addressed.

The flow rates achievable in the laboratory are used to adjust the design discharge employed. Laboratory pumps deliver a maximum discharge Q of about 0.0268 $m^3\ s^{-1}$, which is slightly less than the 0.0302 $m^3\ s^{-1}$ required to simulate a scaled prototype value of $Q_{1.5}$ in the model. This maximum laboratory discharge corresponds to the 1.48-yr return period for the prototype (Fig. 1), which is deemed acceptable to simulate the prototype $Q_{1.5}$. All experimental parameters then are adjusted to this achievable model discharge and summarized in Table 3.

4.2. Movable-bed model design

Movable-bed model design methods parallel those used for the fixed-bed model. Since the movable-bed channel will be created within the fixed-bed model channel, the width is reduced to 1.7 m to allow for construction of a channel with 34° stream banks, as employed by Wallerstein et al. (1999, 2001) and Bennett et al. (2008) (this angle ensures stable side-slopes). These conditions result in a trapezoidal cross-sectional channel geometry with $Y_r = 23.8$ (based on top

Table 3
Summary of prototype and fixed- and movable-bed model dimensions and hydraulic parameters, including relevant scaling ratios for each model. Also included are those parameters used in the actual models.

Parameter	Symbol	Units	Fixed-bed				Movable-bed			
			Prototype	Model design	Scaling ratio	Actual model	Prototype	Model design	Scaling ratio	Actual model
Discharge	Q	$m^3\ s^{-1}$	51.1	0.0268	1907	0.0268	60.2	0.0268	2245	0.0268
Top width	w_T	m	40.5	1.9	21.3	1.9	40.5	1.70	23.8	1.62
Bottom width	w_B	m	40.5	1.9	21.3	1.9	40.5	1.31	30.9	1.31
Depth	h	m	2.2	0.11	20.0	0.11	2.2	0.12	18.3	0.104
Velocity	v	$m\ s^{-1}$	0.574	0.128	–	0.125	0.676	0.148	–	0.176
Bed slope	S_B		0.00047	0.0005	0.94	0.0006	0.00047	0.0006	0.77	0.0006
Hydraulic depth	Y_h	m	2.2	0.11	–	0.11	2.2	0.106	20.7	0.094
Froude number	Fr		0.124	0.124	1	0.124	0.145	0.145	1	0.183
Reynolds number	Re		10^6	10^4	–	10^4	10^6	10^4	–	10^4
Hydraulic radius	R	m	1.98	0.099	20.1	0.099	1.98	0.104	19.1	0.091
Manning's roughness	n	$s\ m^{-1/3}$	0.059	0.037	–	0.042	0.05	0.036	–	0.027
Bank angle	α	deg	90	90	–	90	90	34	–	34
Bed shear stress	τ_0	Pa	8.96	0.48	–	0.58	8.96	0.62	–	0.50
Median particle size	D_{50}	mm	0.08–0.1	–	–	–	0.08–0.1	0.6–1.3	–	0.35

Please cite this article in press as: Gallisdorfer, M.S., et al., Physical-scale model designs for engineered log jams in rivers, Journal of Hydro-environment Research (2013), http://dx.doi.org/10.1016/j.jher.2013.10.002

width), $R_r = 20.4$, $S_r = 0.84$, and $Q_r = 2558.1$ (where $R_m = 0.097$, $S_m = 0.00055$ and $Q_m = 0.0235\ \mathrm{m^3\ s^{-1}}$). Given that maximum discharge is fixed, whose value is 119% of the scaled value of Q_m with $h_m = 0.11$ m and $Z_r = 20.0$, the resulting movable-bed model discharge scaled to the prototype is greater than $Q_{1.5}$. To address this potential discrepancy, h_m is increased to 0.12 m, which leads to a scaled value for Q_p of 60.2 $\mathrm{m^3\ s^{-1}}$ or a 1.61-yr return flow, where R_r, S_r, and Q_r now are 19.1, 0.770, and 2245.1, respectively, with $R_m = 0.104$, $S_m = 0.0006$, and $Q_m = 0.0268\ \mathrm{m^3\ s^{-1}}$. A movable-bed model flow depth of 0.12 m is sufficiently close to the flow depth calculated to simulate $Q_{1.5}$, with $Y_r/Z_r = 1.30$ in the depth-distorted model. Because of the trapezoidal cross-sectional geometry of the movable-bed channel, a hydraulic depth Y_h is defined as $Y_h = A/Y = 0.106$ m, where A is channel cross-sectional area and Y is the channel top width. This hydraulic depth is used to determine the correctly scaled movable-bed model discharge and all appropriate flow conditions (see Wallerstein et al., 1999). Corresponding adjustments are made to all movable-bed parameters and summarized in Table 3.

The bed material used to construct the movable-bed model channel is determined assuming that flow conditions will be just below the threshold of motion. Assuming $\tau_{0m} = 0.62$ Pa (see Table 3 and Eq. (11)), the median grain size of the model bed sediment D_{50m} just below its threshold of motion (a nominal value of 10% less is used) is estimated using Eq. (9) and solving for $D = D_{50c}$, with $\theta_c = 0.03$, 0.045, and 0.060. This calculation produces model bed grain sizes of 0.6–1.3 mm for quartz-density sand, but this must be verified experimentally. Finally, by assuming $D_{50m} = 0.8$ mm, it is necessary to adjust the movable-bed τ_{0m} by varying h_m (and R_m) to empirically determine model flow conditions at or just below the threshold of motion, since S_m is fixed. This is accomplished by varying h_m, and thus R_m, with $h_m \leq m$, which corresponds to Q_p represented by flow conditions in the fixed-bed model, when movable- and fixed-bed Q_m are equivalent and $Q_p = 51.1\ \mathrm{m^3\ s^{-1}}$. In this case, it again is necessary to increase h_m to accommodate the fixed discharge delivered by laboratory pumps. Final movable-bed model scaling design is summarized in Table 3. An undistorted movable-bed model could be designed when materials of reduced density and increased diameter are available to serve as model sediments and where laboratory equipment limitations and space constraints are less restrictive (Julien, 2002). Lastly, the goal of the movable-bed experiment is to evaluate scour

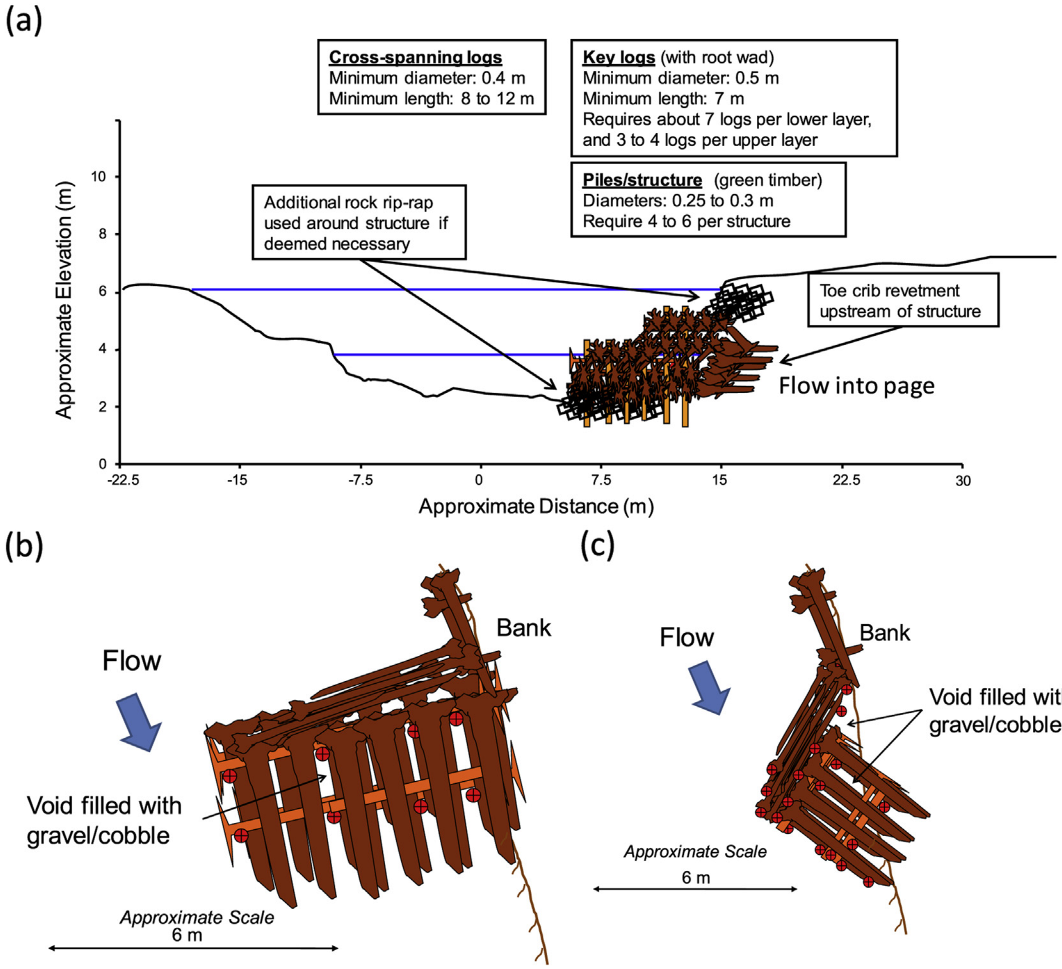
(a)
Cross-spanning logs
Minimum diameter: 0.4 m
Minimum length: 8 to 12 m
Key logs (with root wad)
Minimum diameter: 0.5 m
Minimum length: 7 m
Requires about 7 logs per lower layer, and 3 to 4 logs per upper layer
Piles/structure (green timber)
Diameters: 0.25 to 0.3 m
Require 4 to 6 per structure
Additional rock rip-rap used around structure if deemed necessary
Toe crib revetment upstream of structure
Flow into page
Approximate Elevation (m)
0
2
4
6
8
10
-22.5
-15
-7.5
0
7.5
15
22.5
30
Approximate Distance (m)
(b)
Flow
Bank
Void filled with gravel/cobble
Approximate Scale
6 m
(c)
Flow
Bank
Void filled with gravel/cobble
Approximate Scale
6 m

Fig. 3. Schematic drawings of proposed engineered log jams to be installed along the Big Sioux River, showing (a) cross-section view of a bank-attached deflector jam (ELJ-1), (b) plan-view of ELJ-1, and (c) a plan-view of a bank-attached spur jam (ELJ-2).

Please cite this article in press as: Gallisdorfer, M.S., et al., Physical-scale model designs for engineered log jams in rivers, Journal of Hydro-environment Research (2013), http://dx.doi.org/10.1016/j.jher.2013.10.002

patterns resulting from ELJ models. Because the movement and transport of sediment are not scaled (see Einstein and Chien, 1954), the resulting scour patterns will not simulate exactly the scour occurring in the prototype. The movable-bed scour results therefore are intended to provide a qualitative analogy to scour occurring in the prototype, characterizing its general properties (Maynord, 2006).

4.3. Engineered log jam design

The primary goal of the engineered log jams to be installed along the Big Sioux River is bank protection, and two model designs are proposed. The first, called ELJ-1, is a slightly modified version of a bank-attached deflector jam described by Brooks (2006) (Abbe and Brooks, 2011; Fig. 3a and b). ELJ-1 presents a two-tiered design incorporating prototype elements of variable dimensions related to their role and placement within the structure. Embedded piles anchor ELJs to the channel bed, and these are preferably selected from flexible green timber and have a smaller diameter than the key- and cross-spanning logs. Key- and cross-spanning logs also retain their rootwads, which are oriented either upstream or parallel to the flow, providing the greatest amount of surface area to dissipate energy. The basal key logs typically are buried to a depth greater than the anticipated scour depth, and the height of the structure is at least half the height of the design flow stage. Additional rock rip-rap or wood may be used around the structure in practice, if these are deemed necessary.

The second proposed structure, called ELJ-2, also is a slightly modified version of a bank-attached deflector jam, but shaped like a spur dike (Fig. 3c). The design of ELJ-2 differs from ELJ-1 in that it is a single-tiered design oriented at an angle approximately 45° downstream relative to oncoming flow. Otherwise, ELJ-2 is composed of the same elements, dimensions, and design criteria as ELJ-1.

Constructing models of ELJ-1 and ELJ-2 requires some simplification. These models are constructed entirely from scaled elements of identical dimensions as opposed to differently sized elements representing piles, cross-spanning logs, and key logs. Field data describing the dimensions of local timber are available, with a mean trunk diameter at breast-height D_T of 0.78 m, and a mean log length L_T of 9.54 m (S. Brich, pers. comm.). It is also assumed that rootwad diameter RW_T is equal to $2D_T$, or 1.56 m. Adopting the transverse scale ratio $Y_r = 23.8$ of the movable-bed model results in scaled timber element dimensions of 0.033 m for D_T, 0.066 m for model rootwad diameter RW_T, and 0.401 m for element length L_T. Model elements are constructed from available poplar (Populus spp.) dowel stock, 0.032 m in diameter, and plywood rootwad discs are fabricated to approximate the above-presented dimensions (Table 4).

Scale models of ELJ-1 and ELJ-2 were assembled from these elements. The maximum height for both models is 0.147 m, calculated by summing the heights of individual elements, as assembled in the ELJ crib, and the height of the rootwad disk extending slightly above the structure, which corresponds to a prototype height of 3.49 m, with the lower-tier of ELJ-1 somewhat shorter at 0.115 m (2.74 m for the prototype; Figs. 4 and 5). Model ELJs comprise five layers of elements: three layers of key elements with a diameter of 0.032 m, and two layers of notched, cross-spanning logs with an effective diameter of 0.019 m. ELJ structures were assembled using waterproof adhesive, which caused some minor distortion in the overall dimensions (Figs. 4 and 5, Table 4). Because of this construction, it is assumed that the ELJ will act as a solid body, and that flexure of individual elements or the entire structure is considered negligible. Finally, model ELJ-1 penetrates 0.40 m into flow because of its orientation. Model ELJ-2 penetrates 0.282 m into the flow, as it is cut to 45° using $0.5(L_T)\sqrt{2}$ as a guide to determine this length. ELJ-1 and ELJ-2 would penetrate 9.54 m and 6.71 m, respectively, into the prototype flow (Table 4; Fig. 3a).

5. Physical model implementation and application

With the initial design of the physical models completed, the experimental campaign was implemented. Preliminary methods and results from the physical models are presented and discussed below.

5.1. Fixed-bed methods

The experimental parameters used in the fixed-bed model are summarized in Table 3. Nearly all actual (measured) parameters agree exactly with the design parameters except for flow velocity, which is 2% lower than the design value, and bed slope and bed shear stress, which are 20% higher than the design value. The larger values of bed slope and bed shear stress are due to the difficulty in manually setting the tilt of the flume, as the 0.0001 difference in bed slope between the design and the actual values shown in Table 3 is equivalent to a difference of less than 1 mm over the length of the flume.

Each engineered log jam type was placed by itself into this fixed-bed model. A fully-saturated ELJ was suspended just above the fixed-bed (millimeters) and about 2 mm from the flume wall at a location 4.6 m downstream of the headbox

Table 4
Summary of prototype and fixed -and movable-bed ELJ element dimensions and scaling ratios.

Parameter	Symbol	Units	Prototype	Fixed-bed			Movable-bed	
				Model element	Target width ratio	Actual width ratio	Target width ratio	Actual width ratio
Mean trunk diameter	D_T	m	0.78	0.033	21.3	23.8	23.8	23.8
Mean root diameter	RW_T	m	1.56	0.066	21.3	23.8	23.8	23.8
Element length	L_T	m	9.54	0.401	21.3	23.8	23.8	23.8

Please cite this article in press as: Gallisdorfer, M.S., et al., Physical-scale model designs for engineered log jams in rivers, Journal of Hydro-environment Research (2013), http://dx.doi.org/10.1016/j.jher.2013.10.002

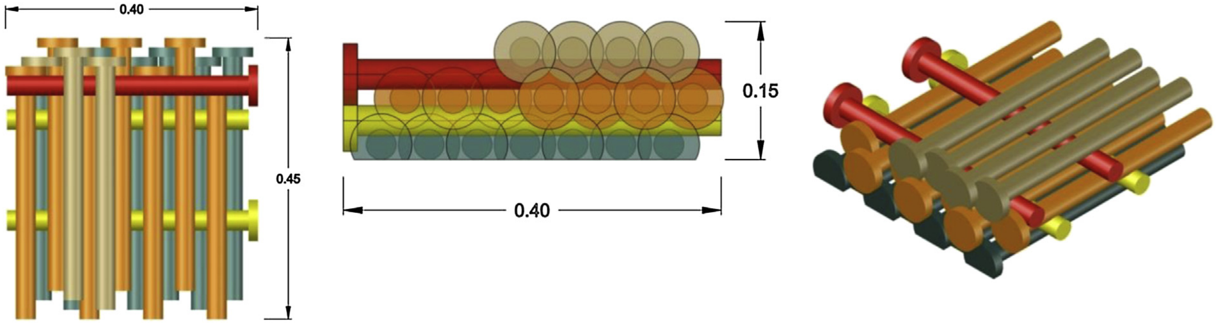

Fig. 4. Model drawings of ELJ-1 showing plan view (left), frontal view (center), and front-right view (right). Dimensions are in meters.

(Fig. 2). The ELJ was suspended pendant to flow and mounted to a FUTEK MBA400 biaxial load cell, which has a maximum dynamic range of 223 N and a resolution of 0.03 N. This configuration allowed fluid forces acting on the instrumented ELJ to be measured in the downstream x and cross-stream y direction. The load cell was carefully calibrated on-site using these same mounts, submerged ELJ structures, and precise static loads. It should be noted that the bulk hydraulic parameters for the flow and ELJ as a single element are in the fully turbulent flow regime, and that the forces measured are for the entire structure rather than individual members. As such, flow through the ELJ and the potential effects of viscous forces within the ELJ are neglected.

Flow data were collected using an acoustic Doppler current meter. For select cross-sections, vertical profiles of fluctuating velocities were recorded at-a-point using a side-looking 3D Nortek Vectrino II. Each cross-section contained 24 vertical profiles, spaced at intervals of 0.05–0.1 m, and 11 vertical locations above the bed, spaced at intervals of 0.01–0.02 m (all sample locations are shown in Fig. 6). At each location, three dimensional turbulent fluctuations in velocity were recorded for 120 s at 75 Hz. Velocity data were processed using the phase-space threshold filter (WinADV 2.029; U.S. Bureau of Reclamation, 2012), and only the time-averaged values for the downstream velocity component v of select cross-sections are presented here. Vertical profiles of the downstream velocity component, Reynolds stress, and turbulent kinetic energy along the flume centerline within the measurement section (not shown here) agreed well with expected distributions for flat-bed boundaries (e.g., Nezu and Nakagawa, 1993), demonstrating that fully developed flow conditions were achieved.

5.2. Fixed-bed preliminary results

Preliminary results from the fixed-bed model are restricted to the downstream component of velocity and the drag force measured for each engineered log jam type. Fig. 6 shows contour plots of the time-averaged velocity component v for the clear-water flow in the measurements sections of the flume, and 0.1 m downstream of ELJ-1 and ELJ-2. Height above the bed z is normalized by flow depth h, distance across the flume y is normalized by flow width w, and time-averaged flow velocity v is normalized by the spatially averaged flow velocity $\langle v \rangle$, defined as:

$$\langle v \rangle = \frac{1}{A}\int_0^w \int_0^h v(z,y)\mathrm{d}z\mathrm{d}y \qquad (16)$$

where A is the cross-sectional area of the flow. It was assumed that downstream flow velocity is zero at the bed and along the flume sidewalls, and that the flow velocity at the water surface

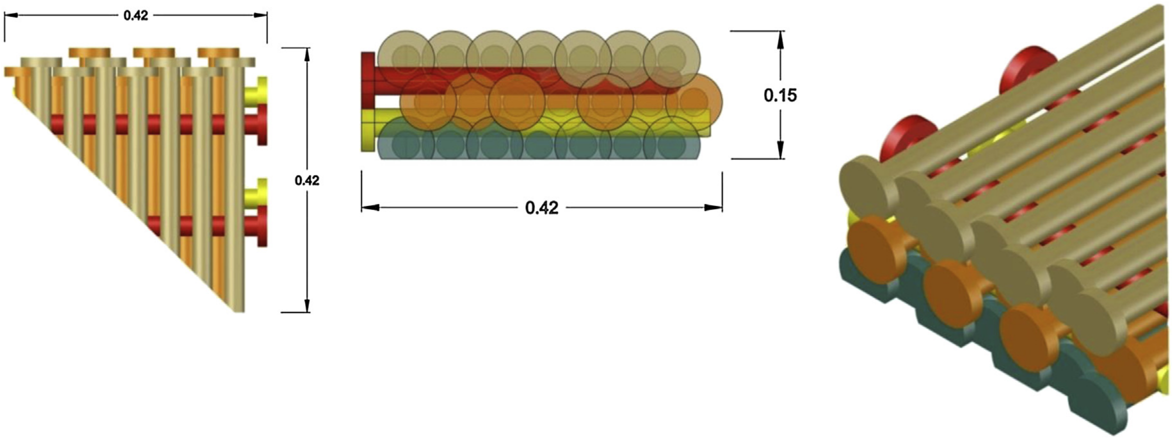

Fig. 5. Model drawings of ELJ-2 showing plan view (left), frontal view (center), and front-right view (right). Dimensions are in meters.

Please cite this article in press as: Gallisdorfer, M.S., et al., Physical-scale model designs for engineered log jams in rivers, Journal of Hydro-environment Research (2013), http://dx.doi.org/10.1016/j.jher.2013.10.002

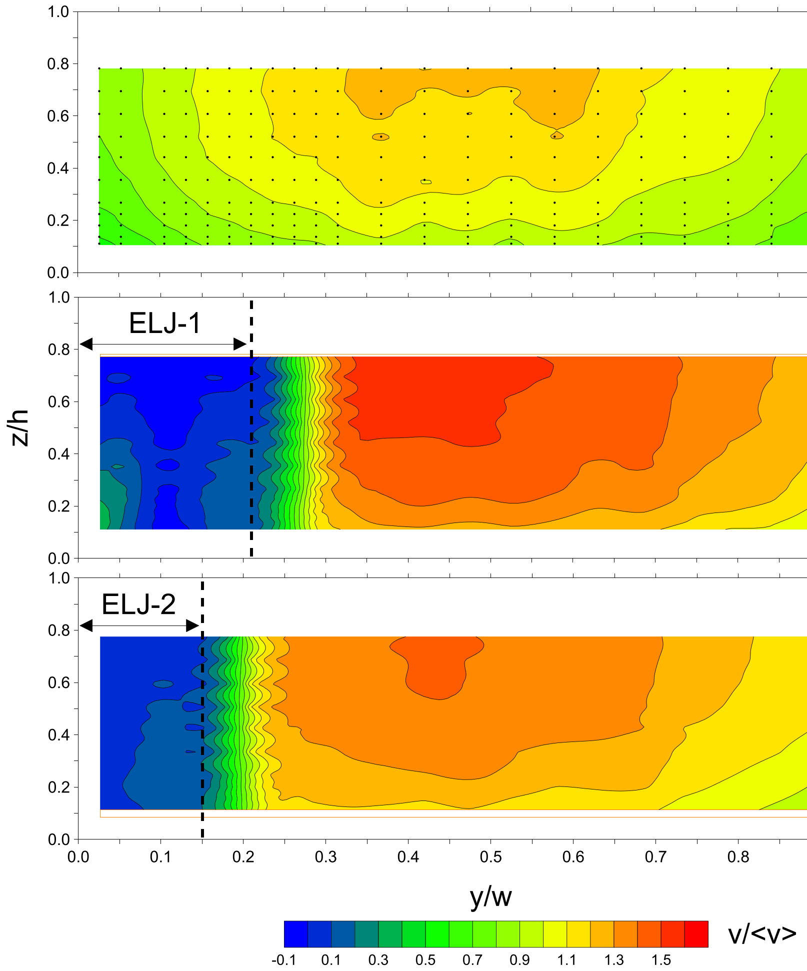

Fig. 6. Contour maps of time-averaged downstream velocity $v$normalized by the spatially averaged velocity $\langle v \rangle$ for the clear-water flow (top; symbols are the sample locations), 0.1 m downstream of ELJ-1 (middle), and 0.1 m downstream of ELJ-2 (lower). The height z above the bed is normalized by flow depth h, the distance y across the flume is normalized by flow width w, and the penetration distance of the ELJs into the flow is shown.

is equal to the flow velocity measured just below the surface. The latter assumption was verified experimentally.

The introduction of the engineered log jams had little effect on spatially averaged flow but a marked effect on localized flow. The spatially averaged flow velocity ($\langle v \rangle = 0.125\ \mathrm{m\ s^{-1}}$) and cross-sectionally averaged flow depth ($h = 0.114$ m) did not change with the addition of the ELJs, either just upstream or just downstream of the structures. Locally, the ELJs created (1) a decelerated flow just downstream of the structure, (2) a vertically oriented mixing layer extending approximately one-half of the structure's width into the flow, and (3) an accelerated flow in the center of the channel that extended to the opposite bank (Fig. 6). Both ELJs effectively created low-velocity zones in the near bank environments, supporting their use as bank protection measures, as observed in natural settings (Daniels and Rhoads, 2003; Manners et al., 2007). While the effect of the ELJs on spatially averaged flow was negligible, localized flow about the structure was significantly modified.

The drag forces acting on each engineered log jam are measurable, and drag coefficients can be derived from these observations. The measured drag forces F_D were 0.85 ± 0.08 N for ELJ-1 and 0.59 ± 0.06 N for ELJ-2 (Table 5). In this application, the cross-stream or transverse forces were, in general, equal to about $0.1F_D$ (not discussed here). From these measurements, a drag coefficient for each structure can be derived using Eq. (15). In this analysis, A_D represents the frontal area of the structure, equal to the structure's penetration distance multiplied by the flow depth (each structure extended to the water surface), whereas v_0 represents the free-stream or incident velocity. Two velocities can be used for v_0: (1) a spatially averaged velocity for the entire clear-water flow, as defined in Eq. (16), and (2) a spatially averaged velocity of the clear-water flow restricted in space to

Table 5
Summary of forces measurements and calculated drag coefficients for each ELJ structure using spatially averaged downstream velocity for the entire flow and that restricted in space incident to structure.

Structure	F_D (N)	Entire flow		Incident to structure	
		$\langle v \rangle$ (m/s)	C_D	$\langle v \rangle$ (m/s)	C_D
ELJ-1	0.85 ± 0.08	0.125	0.30	0.087	0.42
ELJ-2	0.59 ± 0.06	0.125	0.29	0.047	0.78

Please cite this article in press as: Gallisdorfer, M.S., et al., Physical-scale model designs for engineered log jams in rivers, Journal of Hydro-environment Research (2013), http://dx.doi.org/10.1016/j.jher.2013.10.002

the penetration distance of the structure, as quantified by changing the limits of w in equation (16). The drag coefficients based on the spatially averaged velocity for the entire flow are 0.30 for ELJ-1 and 0.29 for ELJ-2, whereas these coefficients increase to 0.42 and 0.78, respectively, using the spatially averaged incident velocity (Table 5). While values of C_D have been reported for single LWD elements (see Wallerstein et al., 2002; Shields and Alonso, 2012), only Gippel et al. (1992) (Shields and Gippel, 1995) reported values for complex (multiple-member) LWD structures, noting that $C_D \approx 0.7$, which is similar to values observed here. Slightly larger values have been used in field applications of ELJs ($\sim$1.2; Brooks, 2006).

5.3. Movable-bed methods

The experimental parameters for the movable-bed model are summarized in Table 3. The sediment used has a median grain size D_{50} of 0.35 mm, chosen because of its local availability. As such, some relaxation of the movable-bed model parameters is required based on experimentation with this sediment.

Initial experimentation focused on optimizing the flow conditions and alluvial response to an introduced ELJ using this sediment. Sand was placed into the flume, and a trapezoidal channel was cut into the moistened sediment (see Table 3; Bennett et al., 2008). With a single ELJ-1 placed into the channel, experiments were conducted by varying the flow depth h from 0.09 to 0.12 m at a flow rate of 0.0268 $m^3\ s^{-1}$. This was done to ensure that that sufficient bed adjustment (erosion) would be observed near the structure within a 24-h period of continuously running the experiment while still maintaining bed stability elsewhere in the channel. A final model flow depth h_m of 0.104 m was selected based on these initial tests, and all movable-bed parameters were revised accordingly (Table 3).

A preliminary movable-bed experiment is presented here. After the sand bed was prepared, the flume was filled with water, flow was initiated, and a single ELJ-1 structure was placed along the sidewall 4.6 m downstream of the headbox. The structure was submerged to a depth of 0.114 m and embedded about 0.01 m into the sand bed. The experiment then ran continuously for 24 h. After this time, the pumps were shut down gradually to preserve the morphologic details of the adjusted channel.

Close-range aerial digital photogrammetry was performed to quantify these channel changes. The system comprises a 10.1 MP Canon EOS Rebel XS camera with a 24 mm lens mounted to a sliding carriage suspended approximately 3.3 m above the channel. Three sets of 13 photographs were taken in-sequence approximately 0.2 m apart, beginning at the downstream end of the flume. A single pre-experiment set captured initial channel topography, and two post-experiment sets captured and confirmed the final channel configuration. Photogrammetry was performed with Photomodeler Scanner, in which the final ground points of the digital elevation model (DEM) exhibited a total mean error of ±1.8 mm. The difference between the pre- and post-experiment DEMs provides a measure of net erosion or deposition within the flume as a result of the ELJ.

5.4. Movable-bed preliminary results

Using the movable-bed model parameters and procedure, morphologic adjustment to the introduction of the single ELJ is presented. Fig. 7 displays an orthophotograph depicting the

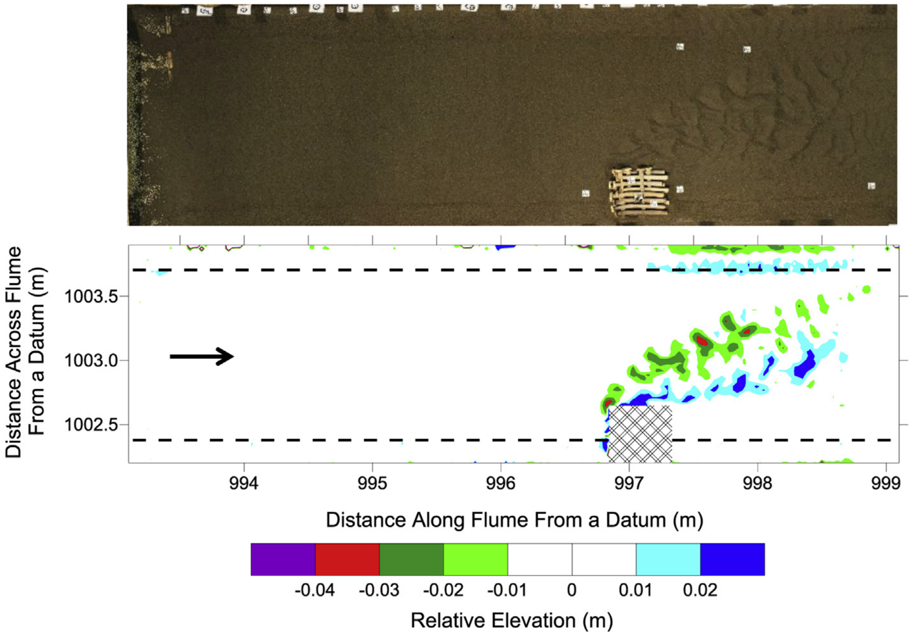

Fig. 7. Channel adjustment to ELJ-1 using the movable-bed model. Orthophotograph (upper) shows ELJ-1 in the channel, with downstream bed adjustment visible (the white squares are used as photogrammetric targets). The contour map (lower) displays the relative erosion (negative values) and deposition (positive values) that occurred in response to introducing ELJ-1 as compared to the prepared channel. In this figure, the textured box is the location of the ELJ, the arrow shows the flow direction, and the dashed lines demarcate the toe of the streambank of the trapezoidal channel.

Please cite this article in press as: Gallisdorfer, M.S., et al., Physical-scale model designs for engineered log jams in rivers, Journal of Hydro-environment Research (2013), http://dx.doi.org/10.1016/j.jher.2013.10.002

entire movable-bed channel, the position of ELJ-1, and visible characteristics of scour resulting from its deployment. Also included in this figure is a contour map of the change in bed surface topography showing net erosion (negative values) and deposition (positive values).

The presence of the ELJ can cause localized erosion and deposition of sediment. The greatest net erosion correlates in space to the position of ELJ-1.This area of bed scour extends from the leading edge of ELJ-1 downstream to the end of the experimental channel, reaching its greatest lateral extent approximately 0.5 m downstream of the structure. The eroded sediment is deposited parallel to and immediately downstream of the scour hole, forming depositional bars. The area of the experimental channel affected by the ELJ, however, is extensive. First, the area of bed erosion and deposition gradually increases with increasing distance downstream, even though the magnitude of the net adjustment decreases. Second, there is measurable bank erosion of and bank-toe deposition near the opposite streambank. These observations suggest that the area of influence for the ELJ is significantly larger than its actual dimensions. Most importantly, no net erosion or deposition is observed along the bank directly downstream of ELJ-1, thus demonstrating its efficacy in bank protection.

These preliminary results show a marked alluvial response to LWD. Svoboda and Russel (2011) also noted that the areas of maximum scour occur where flow rapidly accelerates around the leading edge of a LWD structure, in the center of the channel and downstream of the structure. Yet the ELJ used here, which is a relatively complex structure, produced more erosion of the opposite bank and a larger zone of maximum scour as compared to those experiments that deployed relatively simple LWD designs or single elements (Beschta, 1983; Cherry and Beschta, 1989; Wallerstein et al., 2001; Svoboda and Russell, 2011). This observation may be especially relevant in the deployment of ELJs along the Big Sioux River, where disruption or erosion of the channel's opposite bank is to be avoided (S. Brich, pers. comm.).

6. Concluding remarks

The principles of physical-scale modeling are used to investigate the forces acting upon, and the hydraulic and geomorphic effects of complex ELJs to be installed along the Big Sioux River, SD. Physical models of the prototype are constructed for a selected discharge to evaluate the behavior and effects of two commonly employed ELJ designs. Froude number scaling is appropriate to investigate the hydraulics and morphodynamics of open-channel flows, and it is the preferred approach to scale such river models. Fixed- and movable-bed model dimensions and all hydraulic parameters reflect the resulting scaling ratios for the depth-distorted models, and their derivations are presented and discussed. Relaxation of the Shields parameter and particle Reynolds number scaling ratios for the movable-bed model enables the use of flows, facilities, and materials typically available in research laboratories. These scaling procedures also are applied to the available timber to be used to construct the ELJs in the prototype, and the structures used in the models reflect this scaling. By adopting and applying this scaling procedure, the experimentalist is assured that the results obtained will capture well the hydraulic and morphodynamic response of the prototype to the installed ELJs.

Preliminary results obtained from the physical models illustrate the effects of ELJs on open-channel flow. The ELJs in the fixed-bed model had a measurable effect on localized flow, causing deceleration of flow near the structure and acceleration of flow away from the structure. Yet spatially averaged flow velocity and depth remained the same. Downstream drag forces measured on the ELJs were approximately an order of magnitude larger than the measured cross-stream forces, and drag coefficients varied from 0.3 to 0.7 depending on the velocity scale used. The ELJ in the movable-bed model created areas of localized scour and deposition, yet this zone of influence extended markedly both downstream and across the channel.

Design methods for prototype-scaled physical river models, and especially for creating and evaluating prototype-scaled ELJ models, may be adapted to reflect dimensions and hydraulic parameters of other rivers undergoing restoration. By including complex, multi-element scaled models of ELJs in these experiments, the transferability of experimental results to the prototype will be enhanced and potentially lead to improvements in river restoration design. Physical-scale modeling remains a relevant and viable experimental tool for evaluating ELJ designs, for assessing the potential impacts and outcomes of alternative restoration schemes, and for investigating additional aspects of river and ecosystem restoration.

Acknowledgments

We thank Kevin Cullinan, Tom Gruenauer, and Tim Martz for providing technical assistance during the construction of the flume, Sol Brich for providing much of the background information on the Big Sioux River, and Donghua Cai for helping with the data collection. An earlier version of this paper was reviewed by three anonymous referees and journal editor, who made many helpful suggestions on ways to improve it. This research was financially supported by the City of Sioux Falls, SD, and the USDA-ARS (Specific Research Agreement No. 58-6408-9-346).

References

Abbe, T., Brooks, A., 2011. Geomorphic, engineering, and ecological consideration when using wood in river restoration. In: Simon, A., Bennett, S.J., Castro, J.M. (Eds.), Stream Restoration in Dynamic Fluvial Systems: Scientific Approaches, Analyses, and Tools, Geophysical Monograph 194. American Geophysical Union, Washington, D.C, pp. 419–451.

Abbe, T.B., Montgomery, D.R., 1996. Large woody debris jams, channel hydraulics and habitat formation in large rivers. Regul. Rivers Res. Manage. 12, 201–221.

Abbe, T.B., Brooks, A.P., Montgomery, D.R., 2003a. Wood in river rehabilitation and management. In: Gregory, S.V., Boyer, K.L., Gurnell, A.M. (Eds.), The Ecology and Management of Wood in World Rivers, American Fisheries Society Symposium 37. American Fisheries Society, Bethesda, MD, pp. 367–389.

Abbe, T.B., Pess, G., Montgomery, D.R., Featherston, K.L., 2003b. Integrating engineered log jam technology into river rehabilitation. In: Montgomery, D.R., Bolton, S., Booth, D.B., Wall, L. (Eds.), The Restoration of Puget Sound Rivers. The University of Washington Press, Seattle, pp. 432—470.

Alonso, C.V., 2004. Effects of emergent riparian vegetation on spatially-averaged and turbulent flow within an experimental channel. In: Bennett, S.J., Simon, A. (Eds.), Riparian Vegetation and Fluvial Geomorphology, Water Science and Application Series, vol. 8. American Geophysical Union, Washington, D.C, pp. 59—69.

Alonso, C.V., Shields Jr., F.D., Temple, D.M., 2005. Experimental study of drag and lift forces on prototype scale models of large wood. In: Paper Presented at ASCE World Water and Environmental Resources Congress. American Society of Civil Engineering, Anchorage, Alaska.

Alonso, C.V., Shields Jr., F.D., Temple, D.M., 2009. Dynamics of large wood: a prototype scale flume experiment. In: 33rd IAHR Congress: Water Engineering for a Sustainable Environment, pp. 5151—5158.

Beebe, J.T., 2000. Flume studies of the effect of perpendicular log obstructions on flow patterns and bed topography. Great Lakes Geographer 7, 9—25.

Bennett, S.J., Wu, W., Alonso, C.V., Wang, S.S.Y., 2008. Modeling fluvial response to in-stream woody vegetation: implications for stream corridor restoration. Earth Surf. Processes Landforms 33, 890—909.

Bernhardt, E.S., Palmer, M.A., Allan, J.D., Alexander, G., Barnas, K., Brooks, S., Carr, J., Clayton, S., Dahm, C., Follstad-Shah, J., Galat, D., Gloss, S., Goodwin, P., Hart, D., Hassett, B., Jenkinson, R., Katz, S., Kondolf, G.M.., Lake, P.S., Lave, R., Meyer, J.L., O'Donnell, T.K., Pagano, L., Powell, B., Sudduth, E., 2005. Synthesizing U.S. river restoration efforts. Science 308, 636—637.

Beschta, R.L., 1983. The effects of large organic debris upon channel morphology: a flume study. In: Proceedings of D.B. Simons Symposium on Erosion and Sedimentation, Fort Collins, CO, pp. 8-63—8-78.

Bocchiola, D., Rulli, M.C., Rosso, R., 2006. Flume experiments on wood entrainment in rivers. Adv. Water Resour. 29, 1182—1195.

Bocchiola, D., 2011. Hydraulic characteristics and habitat suitability in presence of woody debris: a flume experiment. Adv. Water Resour. 34, 1304—1319.

Braudrick, C.A., Grant, G.E., Ishikawa, Y., Ikeda, H., 1997. Dynamics of wood transport in streams: a flume experiments. Earth Surf. Processes Landforms 22, 669—683.

Braudrick, C.A., Grant, G.E., 2000. When do logs move in rivers? Water Resour. Res. 36, 571—583.

Braudrick, C.A., Grant, G.E., 2001. Transport and deposition of large woody debris in streams: a flume experiment. Geomorphology 41, 263—283.

Bridge, J.S., Bennett, S.J., 1992. A model for the entrainment and transport of sediment grains of mixed sizes, shapes and densities. Water Resour. Res. 28, 337—363.

Brooks, A., 2006. Design Guideline for the Reintroduction of Wood into Australian Streams. Land and Water Australia, Canberra, 85 p.

Cherry, J., Beschta, R.L., 1989. Coarse woody debris and channel morphology: a flume study. Water Resour. Bull. 25, 1031—1036.

Collins, B.D., Montgomery, D.R., Fetherston, K., Abbe, T.B., 2012. The floodplain large-wood cycle hypothesis: a mechanism for the physical and biotic structuring of temperate forested alluvial valleys in the North Pacific coastal ecoregion. Geomorphology 139—140, 460—470.

Daniels, M.D., Rhoads, B.L., 2003. Influence of a large woody debris obstruction on three-dimensional flow structure in a meander bend. Geomorphology 51, 159—173.

D'Aoust, S.G., Millar, R.G., 2000. Stability of ballasted woody debris habitat structures. J. Hydraul. Eng. 126, 810—817.

Einstein, H.A., Chien, N., 1954. Similarity of distorted river models with movable bed. Proc. Hydraul. Div. Am. Soc. Civil Eng. 80. No. 566.

Flores, L., Larranaga, A., Diez, J., Elosegi, A., 2011. Experimental wood addition in streams: effects on organic matter storage and breakdown. Freshw. Biol. 56, 2156—2167.

Gippel, C.J., O'Neill, I.C., Finlayson, B.L., 1992. The Hydraulic Basis of Snag Management. Centre for Environmental Applied Hydrology, Department of Civil and Agricultural Engineering, University of Melbourne, Parkville, Australia.

Heller, V., 2011. Scale effects in physical hydraulic engineering. J. Hydraul. Res. 49, 293—306.

Henderson, F.M., 1966. Open Channel Flow. MacMillan, New York, 522 p.

Julien, P.Y., 2002. River Mechanics. Cambridge University Press, Cambridge, 434 p.

Manners, R.B., Doyle, M.W., Small, M.J., 2007. Structure and hydraulics of natural woody debris jams. Water Resour. Res. 43, W06432. http://dx.doi.org/10.1029/2006WR004910.

Maynord, S.T., 2006. Evaluation of the micromodel: an extremely small-scale movable-bed model. J. Hydraul. Eng. 132, 343—353.

Mutz, M., Kalbus, E., Meinecke, S., 2007. Effect of instream wood on vertical water flux in low-energy sand bed flume experiments. Water Resour. Res. 43, W10424. http://dx.doi.org/10.1029/2006WR005676.

Naudascher, E., 1984. Scale effects in gate model tests. In: Kobus, H. (Ed.), Symposium on Scale Effects in Modelling Hydraulic Structures. International Association for Hydraulic Research, DeutscherVerbanfuerWasserwirtschaft und Kulturbau e. V., Esslingen am Neckar, Germany. § 1.1.

Nezu, I., Nakagawa, H., 1993. Turbulence in Open-Channel Flows. A.A. Balkema, Rotterdam, 286 p.

Pugh, C.A., 2008. Sediment transport scaling for physical models. In: Garcia, M.H. (Ed.), Sedimentation Engineering, Processes, Measurements, Modeling, and Practice, ASCE Manuals and Reports on Engineering Practice, No. 110. ASCE, Reston, VA, pp. 1057—1065.

Shields Jr., F.D., Alonso, C.V., 2012. Assessment of flow forces on large wood in rivers. Water Resour. Res. 48, W04516. http://dx.doi.org/10.1029/2011WR011547.

Shields Jr., F.D., Gippel, C.J., 1995. Prediction of effects of woody debris removal on flow resistance. J. Hydraul. Eng. 121, 341—354.

Shields Jr., F.D., Morin, N., Cooper, C.M., 2004. Large woody debris structures for sand bed channels. J. Hydraul. Eng. 130, 208—217.

Shields Jr., F.D., Pezeshki, S.R., Wilson, G.V., Wu, W., Dabney, S.M., 2008. Rehabilitation of an incised stream with plant materials: the dominance of geomorphic processes. Ecol. Soc. 3. Article 54.

Svoboda, C.D., Russel, K., 2011. Large wood structures for scour development and habitat. In: World Environmental and Water Resources Congress 2011: Bearing Knowledge for Sustainability. ASCE, pp. 2572—2581.

U.S. Bureau of Reclamation, 2012. WinADV 2.029. Available at: http://www.usbr.gov/pmts/hydraulics_lab/twahl/winadv/ (accessed 13.03.2013).

U.S. Bureau of Reclamation and U.S. Army Corps of Engineers, February, 2012. Large Wood Research Workshop Summary Report. Seattle, WA, Report Number: SRH-2012-20, 44 p.

Wallerstein, N.P., Alonso, C.V., Bennett, S.J., Thorne, C.R., 1999. An Experimental Study of Alluvial Channel Response to Large Woody Debris, Research Report No. 10. Channel and Watershed Processes Research Unit, National Sedimentation Laboratory, Oxford, Mississippi 38655, 85 p.

Wallerstein, N.P., Alonso, C.V., Bennett, S.J., Thorne, C.R., 2001. Distorted Froude scaled flume analysis of large woody debris. Earth Surf. Processes Landforms 26, 1265—1283.

Wallerstein, N.P., Alonso, C.V., Bennett, S.J., Thorne, C.R., 2002. Surface wave forces acting on submerged logs. J. Hydraul. Eng. 128, 353—449.

White, F.M., 1994. Fluid Mechanics, third ed. McGraw-Hill, New York. 736 p.

Wilcox, A.C., Wohl, E.E., 2006. Flow resistance dynamics in step-pool channels: 1. Large woody debris and controls on total resistance. Water Resour. Res. 42, W05418. http://dx.doi.org/10.1029/2005ER004277.

Wilcox, A.C., Nelson, J.M., Wohl, E.E., 2006. Flow resistance dynamics in step-pool channels: 2. Partitioning between grain, spill, and woody debris resistance. Water Resour. Res. 42, W05419. http://dx.doi.org/10.1029/2005WR004278.

Yalin, M.S., 1971. Theory of Hydraulic Models. Macmillan, New York, 266 p.

Young, W.J., 1991. Flume study of the hydraulic effects of large woody debris in lowland rivers. Regul. Rivers Res. Manage. 6, 203—211.

Please cite this article in press as: Gallisdorfer, M.S., et al., Physical-scale model designs for engineered log jams in rivers, Journal of Hydro-environment Research (2013), http://dx.doi.org/10.1016/j.jher.2013.10.002

List of variables

A: channel cross-sectional area;
A_D: projected frontal area of structure;
C_D: Drag coefficient;
D: sediment grain diameter;
D_{50}: median sediment grain diameter;
D_T: mean trunk diameter;
F_D: Drag force;
Fr: Froude number;
g: acceleration due to gravity;
h: flow depth;
k_{ELJ}: surface roughness of the ELJ;
L: length;
L_S: height of ELJ relative to water depth;
L_T: ELJ element length;
M: mass;
n: Manning's roughness;
Q: discharge;
$Q_{1.5}$: 1.5 year return flow;
$Q_{2.33}$: 2.33 year return flow;
Q_{ma}: mean annual discharge;
R: hydraulic radius;
Re: Reynolds number;
Re_g: particle Reynolds number;
RW_T: mean rootwad diameter;
S: slope;
S_B: channel-bed slope;
S_S: water surface slope;
T: time;
u^*: shear velocity;
v: velocity;
v_0: incident velocity;
w: width;
w_B: bottom width;
We: Weber number;
w_T: top width;
X, x: longitudinal length;
Y, y: transverse length;
Y_h: hydraulic depth;
Z, z: vertical length;
α: bank angle;
γ: specific weight of water;
β: orientation of the ELJ with respect to flow direction;
γ_s: specific gravity of sediment minus 1;
δ: surface tension;
θ: Shields parameter;
η: porosity of the ELJ;
μ: molecular fluid viscosity;
ξ: specific gravity of sediment;
ρ: fluid density;
τ_0: bed shear stress;
σ: sediment density;
c: threshold conditions;
m: model parameter;
p: prototype parameter;
r: ratio of prototype parameter to model parameter.

Please cite this article in press as: Gallisdorfer, M.S., et al., Physical-scale model designs for engineered log jams in rivers, Journal of Hydro-environment Research (2013), http://dx.doi.org/10.1016/j.jher.2013.10.002